Scientific Contributions Oil & Gas, Vol. 48. No. 4, December: 357 - 375

SCIENTIFIC CONTRIBUTIONS OIL AND GAS

Testing Center for Oil and Gas
LEMIGAS

Journal Homepage:http://www.journal.lemigas.esdm.go.id
ISSN: 2089-3361, e-ISSN: 2541-0520

Porosity-Controlled Flow Instability and Vibration Response in Conical Strainers: An Integrated Hydraulic-Structural Evaluation

Amnur Akhyan[1], Mohd Azahari Bin Razali[1], Hendriko[2], Shahruddin Bin Mahzan[1], Iman Fitri Bin Ismail[1]

[1]Fakulti Kejuruteraan Mekanikal dan Pembuatan, Universiti Tun Hussein Onn Malaysia,
86400 Parit Raja, Batu Pahat, Johor, Malaysia.

[2]Program Studi Teknik Rekayasa Mekatronika,Jurusan Teknologi Industri, Politeknik Caltex Riau,
Umbansari Street 1 Rumbai, Pekanbaru, Riau, Indonesia, 28285.

Corresponding Author : Mohd Azahari Bin Razali (azahari@uthm.edu.my)

Manuscript received: October 31th, 2025; Revised: November 17th, 2025
Approved: December 15th, 2025; Available online: December 30th, 2025; Published: December 30th, 2025.

ABSTRACT - Research on how porosity can trigger vibrations due to flow-induced instability (FIV) partially clogged in perforated conical strainer has been conducted integrated experimental. Six conical filters with porosities between 25 and 40 percent, made in straight and staggered perforation patterns, were tested under clean and clogged conditions using a set of tools with a controlled closed-loop flow. Pressure drop, vibration amplitude, and frequency were measured simultaneously to capture the coupled hydraulic-structural response. The results show that the straight configuration with low porosity exhibits strong geometric constriction, which accelerates the formation of the jet flow, increases turbulence intensity, and strengthens the vibration amplitude as blockage increases. Conversely, strainers with a minimum porosity of 30 percent and staggered holes promote more uniform flow distribution, reduce shear layer instability, and result in a more stable frequency response. The effect of pressure drop on vibration confirms that clogged can lead to dynamic instability of the system, particularly in high-risk frequency bands common in piping facilities. These experimental results are highly relevant to oil and gas exploration and exploitation activities during drilling, well testing, and production operations. Where fluctuating flow rates, entrained solids, and increased clogging are unavoidable. These findings provide practical guidance for determining the porosity of conical strainers and the perforation layout to reduce hydraulic losses, mitigate vibration damage, and improve the operational reliability of piping systems in oil and gas facilities.

Keywords: conical strainers, porosity, flow-Induced vibration (FIV), clean and clogging conditions.

How to cite this article:

Amnur Akhyan, Mohd Azahari Bin Razali, Hendriko, Shahruddin Bin Mahzan, Iman Fitri Bin Ismail 2025, Porosity-Controlled Flow Instability and Vibration Response in Conical Strainers: An Integrated Hydraulic-Structural Evaluation, Scientific Contributions Oil and Gas, 48 (4) pp. 357 - 375. DOI org/10.29017/scog.v48i4.1960.

INTRODUCTION

One of the critical filtration elements in oil and gas pipeline systems is the conical strainer, which serves to protect downstream equipment from particulate contamination. Its hydraulic performance and vibration response are strongly governed by geometric parameters such as perforation pattern, cone angle, and porosity (Fang et al., 2024; Yin et al., 2024). Recent studies have found that pressure drop (ΔP), turbulence intensity, and resistance to clogging are directly influenced by orifice arrangement and the selection of the open area ratio (OAR). And ultimately, this will impact hydraulic efficiency and mechanical stability (Akhyan et al., 2025; Puderbach et al., 2021; H. Wang et al., 2022). Porosity can be defined as the ratio of the open flow area to the total surface area of the filter. Porosity plays an important role in the interactions in this study. Although higher porosity generally reduces pressure loss, it also modifies local turbulence structures that can intensify flow instabilities and vibration amplitudes. Experimental and numerical (Bon et al., 2024; Wayo et al., 2022) results show that conical screens with an open area ratio of approximately 30–40% provide better flow uniformity and lower clogging rates compared to low porosity configurations.

Flow-induced vibration (FIV) analyses further show that non-uniform flow features such as vortex shedding and recirculation zones arise from geometric discontinuities, including perforations and the conical transition, producing periodic oscillations within the fluid–structure system (Bon et al., 2024; Hamzah et al., 2021; Wayo et al., 2022). Under fluid–structure interaction (FSI) conditions, unbalanced hydrodynamic forces acting on the strainer walls can trigger structural vibrations. At the beginning of the blockage, increased mass and damping can shift the natural frequency and place the system within the resonance band. This can occur when the excitation frequency is parallel to a specific flow velocity (Emmerson et al., 2020; T. Wang & Li, 2025). The cause of this alternating clogging and unclogging cycle is the clogging process itself, which is highly dependent on pore geometry and local shear stress (Bon et al., 2024; Y. Zou et al., 2024). Both experimental and numerical findings consistently show that porosity values near 40% minimize pressure loss while maintaining stable flow, strongly influenced by filter orientation and cone angle (Akhyan et al., 2025; Rianto et al., 2025). Research on porous media and subsurface flow indicates that porosity and permeability significantly influence filtration behaviour and pressure dynamics (Widarsono, 2022). High-frequency oscillations are affected by partial blockage, leading to reduced hydraulic performance and increased structural fatigue. This naturally has an impact on reducing the lifespan of components (Ergut, 2025; Harper et al., 2024). Borehole experiments support the previous statement emphasizing the need to optimize porosity and perforation patterns in engineering designs that impact pressure fluctuations and are directly correlated with vibration amplitude (Qing et al., 2006).

This study examines vibration and blockage factors caused by fluid flow. Fluid flow is influenced by several variations in porosity (25%-40%) and perforation patterns (straight and staggered) that occur in conical screens. This phenomenon is frequently observed in oil and gas pipeline systems, where unstable flow behaviour can lead to significant structural vibrations (Fuad et al., 2019). Typically, increased vibrations are caused by partial blockages. Previous studies have found that the hydraulic and geometric characteristics of strainers play a significant role in generating pressure distribution, turbulence intensity, and filtration stability within piping systems (Mahajan & Maurya, 2020). Recent advancements in FSI analysis also emphasize that the perforated configuration affects pressure loss and flow instability, requiring proper modelling and experimental validation (Li et al., 2023). Additionally, a more in-depth evaluation was conducted to understand the dynamic performance and fatigue resistance of the filtration components due to the elastic response and structural vibration integrity of perforated stainless steel under flow excitation conditions (Mironovs et al., 2025).

Although previous researchers have studied this, they investigated the phenomenon separately. This research is novel due to its integrated experimental

approach, which simultaneously tests variations in porosity, perforation patterns, clogging factors (CF), and flow-induced vibration (FIV) behaviour. The lack of interconnected investigation of each parameter in this study is a gap that paves the way for similar investigations in the future. Additionally, the existing literature provides very little discussion on how the evolution of blockage can alter vibration amplitude and frequency response, particularly in conical filters operating under dynamic flow conditions such as those found in oil and gas pipeline flow. This research provides useful knowledge about the fluid-structure interaction mechanisms that affect the dynamic reliability and performance of conical screens by linking these characteristics thru experimental studies. Hopefully, with this finding, the understanding of filter design optimisation, particularly for conical filters, can be improved. And equally important, this can improve operational stability and maintenance strategies for oil and gas pipeline systems.

This experimental method can be suggested as validation for the CFD-FEA method, which is a structural modelling approach. The goal is to reduce structural fatigue caused by vibration and optimise filtration efficiency in complex fluid transport systems.

METHODOLOGY

Experimental setup and flow system Design

The experiment was built by adopting the operational environment of hydrocarbon flow in oil and gas pipeline systems, which uses a closed-loop water circulation system in the Politeknik Caltex Riau fluid laboratory. The test apparatus has several main parts, as shown in Figure 1, including a 3-inch diameter galvanised steel pipe as the fluid channel, and a conical strainer holder. A 6.5 HP centrifugal pump produces a constant volumetric flow rate between 15 and 30 cubic meters per hour and is suitable for turbulent flow regimes of water at room temperature 25°C. The by pass flow is designed so that the volumetric flow rate can be controlled using valves and rotameters as regulators and monitors. The frame is designed to reinforce the test pipe assembly so that it is not affected by external vibrations. Part List: 1). Conical strainer; 2). Pressure gauge upstream; 3). Pressure gauge downstream; 4). Impurities input; 5). Ball valve; 6).

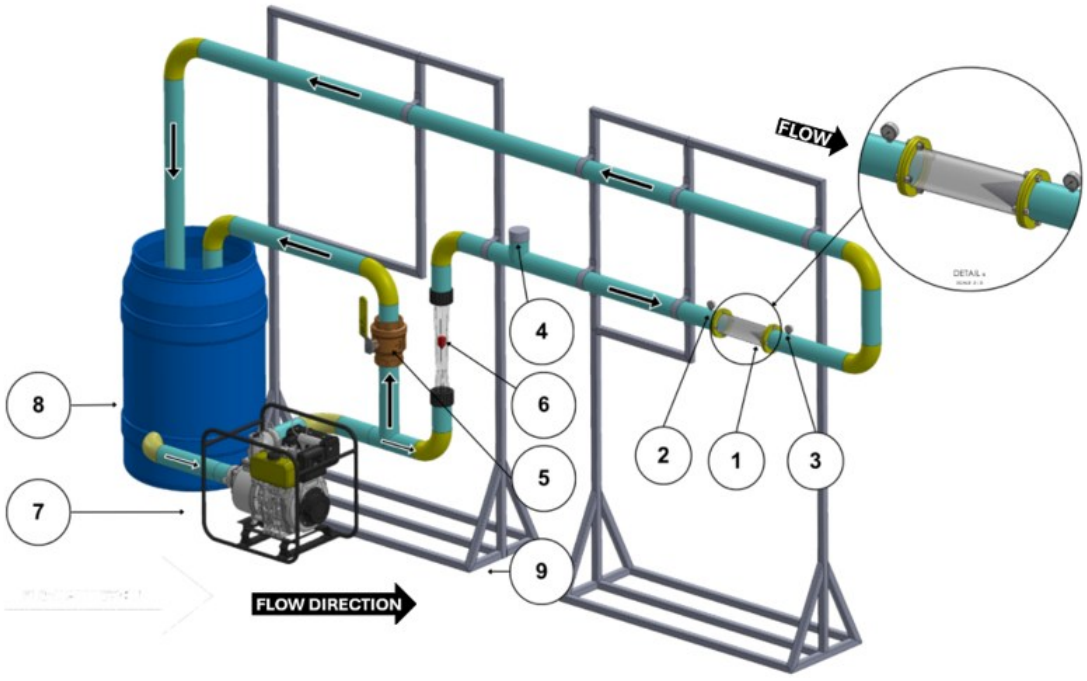

Figure 1. Experimental setup

Rotameter; 7). Pump; 8). Tank; 9). Supporting Frame.

Pressure measuring instruments are placed at the upstream and downstream ends of the conical screen. The upstream pressure gauge is positioned $2D$ to $3D$ before the conical screen, and the downstream pressure gauge is positioned $3D$ to 4D after the conical screen (where D is the inner diameter of the pipe). As shown in Figure 2. The placement of these pressure-measuring instruments complies with flow measurement and filtration testing standards (Mechanical Vibration – Requirements for Instruments for Measuring Vibration Severity, 2012; Qiao et al., 2023). The test fluid is water with welding slag particles as a contaminant. The size of the contaminants is sorted according to the diameter of the conical strainer holes (3 mm, 4 mm, and 6 mm) to achieve consistent clogging in each test. Vibration detection measuring instruments were placed in three positions: upstream, downstream, and exactly in the middle of the conical screen, in order to monitor vibrations along the piping system.

Strainer Geometry and Porosity Variation

In figure 3, there are six conical strainers were fabricated from carbon steel with a wall thickness of 2 millimeters. The strainers differed in perforation pattern (straight or staggered) and hole diameter (3 mm, 4 mm, and 6 mm), producing porosity levels between 25 and 40 per - cent. Porosity (β) is the ratio of the area of open space (holes) to the total surface area of the conical strainer on a local scale. Porosity (β) in Table 2 is calculated using equation 1.

$$\beta = \frac{A_0}{A_t} x100\% \quad (1)$$

A_o is the total open area of the perforations and A_t is the total lateral area of the conical surface. β can be directly obtained from the equation ($90.69\ d^2/p^2$) (Carlomagno et al., 2012) for a staggered pattern and ($78.5\ d^2/p^2$) for a straight pattern, where d is the hole diameter and p is the distance between holes. The geometric configuration was chosen based on previous experimental optimisation work (Akhyan et al., 2025) and supported by the theoretical correlation between porosity and pressure loss (Rianto et al., 2025). As shown in Table 2, this variation allows for evaluating the influence of porosity and perforation pattern on hydraulic performance and vibration behaviour under identical flow conditions.

Table 1. Fluid properties and experimental parameters

Property	Symbol	Value	Unit	Description
Density	ρ	997	kg/m^3	Water at 25° C
Dynamic viscosity	μ	$8{,}9 \times 10^{-4}$	$Pa \cdot S$	Water at 25° C
Temperature	T	25	°C	Ambient test temperature
Flow Rate	Q	15–30	m^3/h	Controlled by a valve and measured using a rotameter
Reynolds number	Re	Turbulent	–	Based on the calculated $Re > 4000$
3D Vibration meter tester. a. Velocity (true RMS) b. Acceleration c. Displacement (peak-peak)	 v(t) a(t) x(t)	 0.01 – 400 0.1 – 400 0.001 – 4	 mm/s m/s^2 mm	VM-6380 vibration meter is in accordant with ISO 2954:2012 [21], Level of accuracy ±5% of reading + 2 digits
Pressure Gauge	–	0 – 0.1	bar	Level of accuracy, C.L. 2.5 (±2.5% FS) EN 837-1:1996 [22]
Rotameter	–	12 – 60	m^3/h	Level of accuracy, ±2% FS (±1.2 m^3/h) ISO 10790:2015 [23]

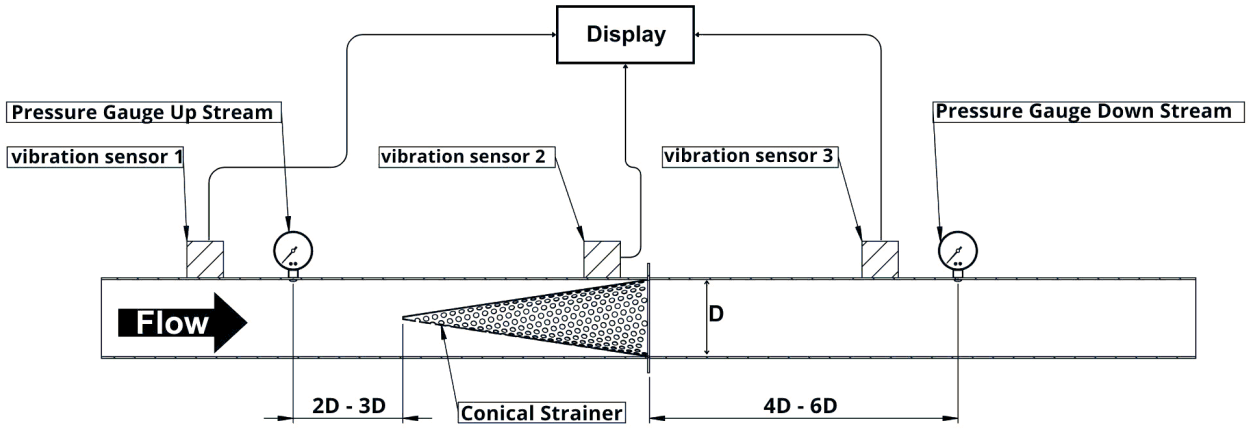

Figure 2. Placement of pressure measuring instruments and vibration sensors

Experimental procedure

The experiment investigates and analyses dynamic performance, in this case, vibrations caused by fluid-induced vibration (FIV) in a conical screen under various flow conditions and blockage levels. The piping system in this experimental study uses a closed pipe system. The complete steps of the experimental procedure are shown in Figure 4.

Testing began by setting a controlled and steady flow rate using a bypass flow and valves. Next, the pressure drop and vibration parameters, such as speed, acceleration, and displacement, were measured using clean water, as shown in Figure 2. This vibration data will be processed to obtain the amplitude and frequency values.

Then, contaminants were introduced, and pressure drop and vibration measurements were taken again. Testing continued until the pressure difference before and after the conical filter reached a maximum and stable value, indicating a constant clogging condition. At this phase, vibration data is obtained simultaneously with flow pressure measurements.

The volumetric flow rate Q It is monitored by a rotameter that has been calibrated to an accuracy of ± 1 percent of full scale. The pressure difference between the upstream and downstream sides of the filter is measured by a Bourdon-type pressure gauge with an accuracy of ± 0.25 percent. Meanwhile, vibration data such as acceleration, velocity, and displacement is monitored by the VM-6380 vibration meter. Each test was conducted under steady-state conditions at different volumetric flow rates at time intervals of 6, 9, 12, 15, and 18 seconds.

Vibration parameter

Vibration measurements in this study refer to the general guidelines provided in (Inservice Testing of Pumps in Light-Water Reactor Power Plants, 2022) and (Mechanical Vibration – Evaluation of Machine Vibration by Measurements on Non-Rotating Parts – Part 3: Industrial Machines with Nominal Power above 15 KW and Nominal Speeds between 120 r/ Min and 15 000 r/Min When Measured in Situ, 2022) standards, which offer several criteria for evaluating the magnitude of vibration amplitude values and the frequency response behaviour of equipment. Vibration data, the amplitude and frequency can be calculated using equations 2.

$$A = \frac{v(t)}{2\pi f} \quad (2)$$

And the acceleration was obtained from $a(\mathrm{t})$ $=(2\pi \mathrm{f})$ 2A There is no standardisation regarding vibration value limits because the general values used in the industry should not be used in fixed standards, . (Shady et al., 2022). Similarly, (Chu et al., 2024) highlight that vibration control relies on keeping the frequency from exceeding the structure's natural frequency to prevent resonance and fatigue.

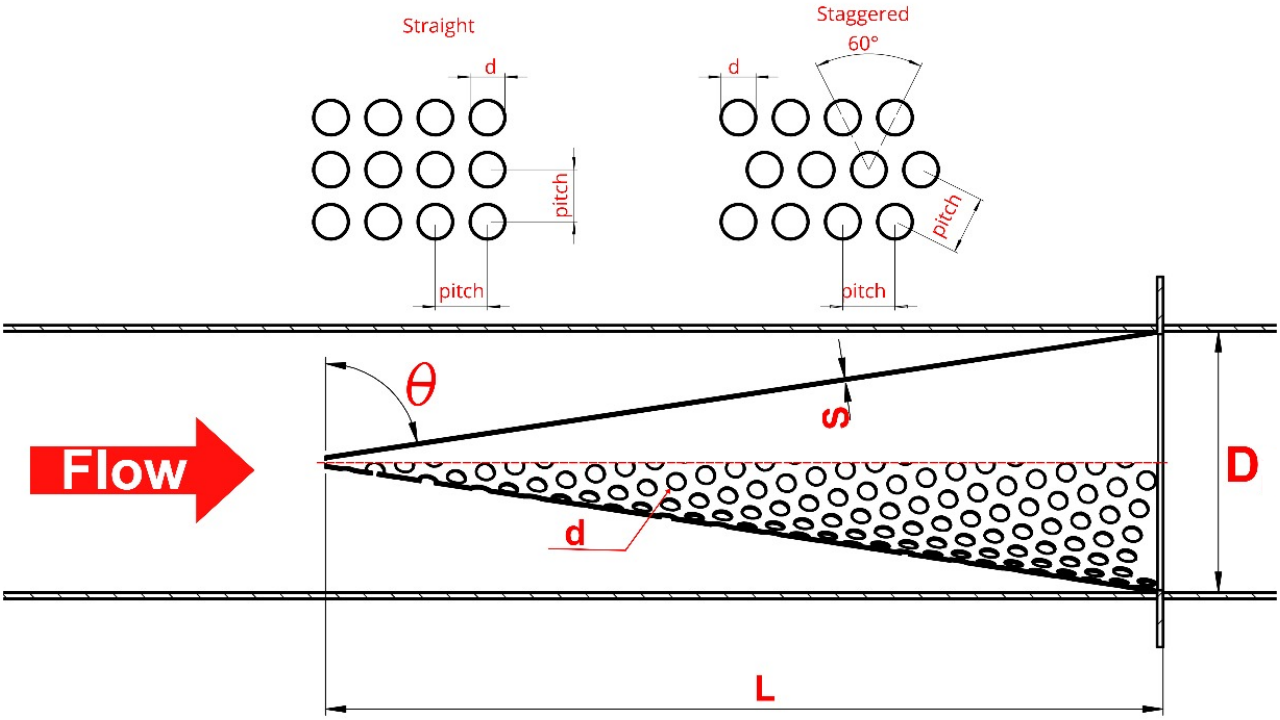

Figure 3. Strainer geometry with the hole pattern and manufacturing results

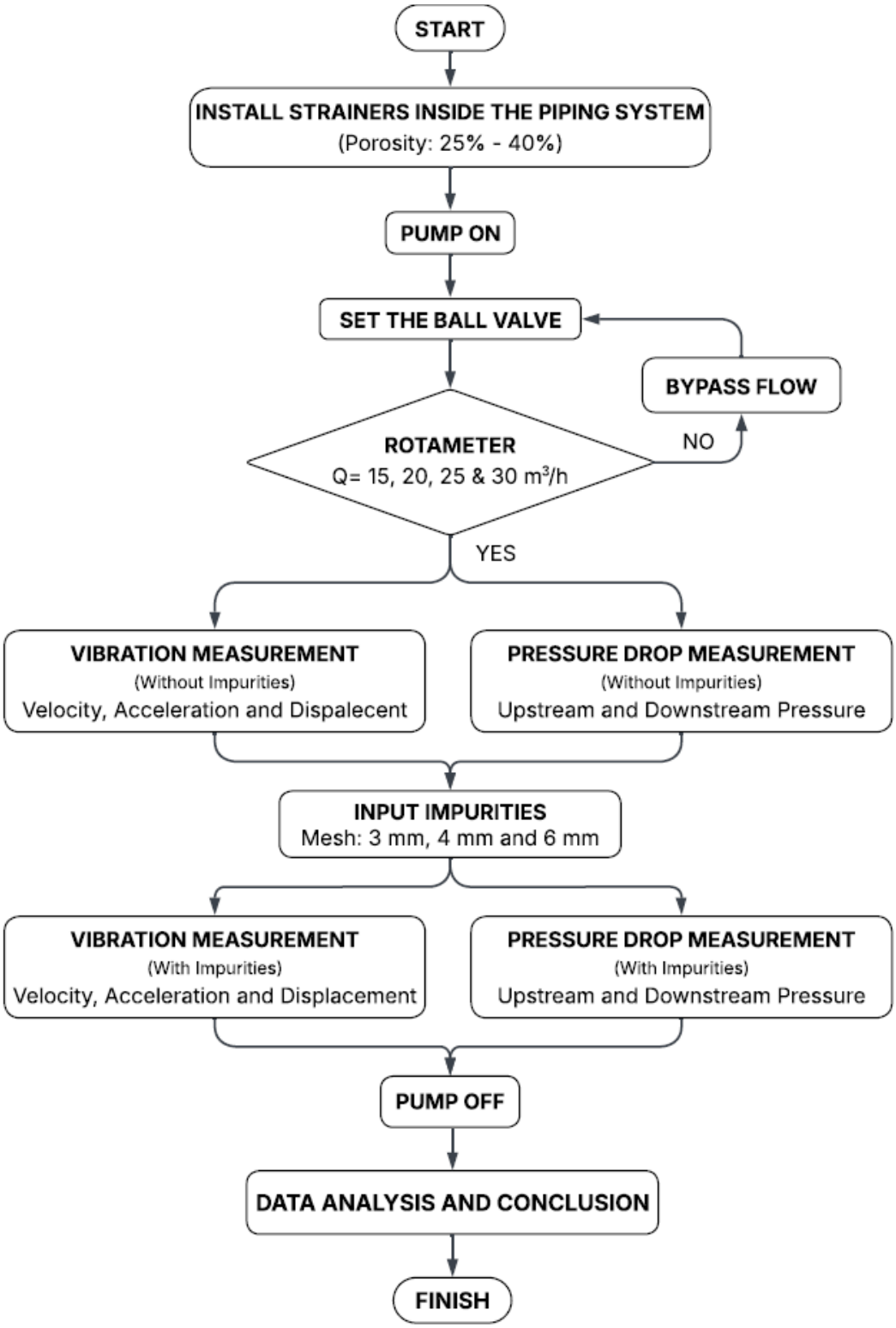

Figure 4. Workflow of experiments

Table 2. Strainer geometry and porosity variation

Hole pattern	Hole diameter, d (mm)	Pitch, p (mm)	Cone angle, θ (Deg)	β Porosity, (%)
Staggered/ Straight	3/3	5/5	74/74	33/28
	4/4	7/7	81/81	30/25
	6/6	9/9	81/81	40/35

Clogging factor (CF)

The ratio between the pressure drop under clogged conditions (ΔPclog) and unclogged (ΔPclean) is also called the clogging factor (CF) (Eker, 2014; Segismundo et al., 2017; Suhaib & Bhunia, 2023), as shown in equation 3. This clogging factor has been adopted for the filtration performance system.

$$CF = \frac{\Delta P_{clog}}{\Delta P_{clean}} \quad (3)$$

The CF value is used to measure the degree of blockage on the surface of the cone strainer due to the accumulation of solid particles and increased flow resistance during data acquisition. There are no standards like (ISO, API, or ASME) that set thresholds for the CF.

RESULT AND DISCUSSION

Vibration response influenced by porosity (β) and pressure drop (ΔP)

The characteristics of vibration due to changes in flow patterns and pressure distribution are influenced by the porosity within the filtration element, such as in a conical strainer. This variation in porosity results in turbulence levels and fluid generation forces that can lead to increased vibration amplitude and frequency.

Table 3 presents data on amplitude (A), frequency (f) and pressure drop influenced by variations in porosity, perforation pattern, and flow rate under both clean and clogged conditions.

Vibration amplitude (A) in clean and clogged condition

A clean condition is a condition where the data taken is from before any contaminants were introduced into the piping system. The data to be examined in this section is the influence of porosity on the amplitude and frequency of vibration under clean conditions, as shown in Figure 5. This clogged condition occurs because debris is introduced into the fluid flow in the test equipment. The debris consists of sorted and introduced welding slag, which is added to the fluid flow after it reaches the desired flow rate and steady-state conditions. The sewage inlet is located upstream of the conical strainer, as shown in Figure 1.

Figure 5. The effect of β and ΔP to A under clean and clogged conditions. Amplitude consistently increases with increasing pressure drop. Under clogged conditions, the response is more dominant than under clean conditions due to the intensification of hydrodynamic forces.

Figure 5 shows that the filter, with its high porosity (β ≈ 40%), consistently maintains lower pressure drops and smaller vibration amplitudes in both clean and clogged conditions. This reinforces the fact that porosity is a key factor influencing hydrodynamic forces. In contrast, a low porosity configuration (β ≈ 25–30%) leads to a sharp increase in flow contraction (turbulence), significant changes in ΔP, and strong vibrations, ultimately impacting fatigue and shortening lifespan (X. Zou et al., 2023). Although the geometry of the hole pattern (staggered vs. straight) affects the uniformity of flow, its influence is not dominant compared to the significant impact of porosity. The increased amplitude under blocked

Table 3. Vibration amplitude due to porosity and pressure drop : clean and clogged conditions

Q (m³/h)	ΔP_{clean} (Pascal)	ΔP_{clog} (Pascal)	A_{clean} (mm)	A_{clog} (mm)	f_{clean} (Hz)	f_{clog} (Hz)	ΔP_{clean} (Pascal)	ΔP_{clog} (Pascal)	A_{clean} (mm)	A_{clog} (mm)	f_{clean} (Hz)	f_{clog} (Hz)
Pressure Drop (ΔP) and Amplitude (A) data ($d = 3$ mm, $p = 5$ mm, dan $\theta = 74°$)												
	Staggered ($\beta = 33\%$)						Straight ($\beta = 28\%$)					
15	25,000	37,500	0.093	0.098	46.92	47.71	27,500	50,000	0.104	0.108	48.89	50.55
20	37,500	50,000	0.096	0.102	47.95	48.63	37,500	62,500	0.110	0.116	49.41	51.16
25	50,000	62,500	0.101	0.109	48.92	49.94	50,000	75,000	0.118	0.124	50.31	52.19
30	62,500	75,000	0.108	0.117	50.92	51.87	75,000	102,500	0.125	0.132	54.59	55.24
Pressure Drop (ΔP) and Amplitude (A) data ($d = 4$ mm, $p = 7$ mm, dan $\theta = 81°$)												
	Staggered ($\beta = 30\%$)						Straight ($\beta = 25\%$)					
15	12,500	15,000	0.080	0.090	36.42	39.17	27,500	37,500	0.101	0.103	39.49	40.57
20	15,000	25,000	0.090	0.102	39.55	41.96	37,500	50,000	0.104	0.107	41.91	43.56
25	25,000	375,00	0.102	0.114	42.00	44.52	50,000	62,500	0.108	0.118	45.15	48.11
30	37,500	50,000	0.114	0.128	47.74	48.19	62,500	75,000	0.117	0.130	48.75	52.93
Pressure Drop (ΔP) and Amplitude (A) data ($d = 6$ mm, $p = 9$ mm, dan $\theta = 81°$)												
	Staggered ($\beta = 40\%$)						Straight ($\beta = 35\%$)					
15	12,500	15,000	0.070	0.078	34.91	39.54	15,000	17,500	0.080	0.087	37.88	41.15
20	15,000	17,500	0.076	0.085	36.75	40.15	17,500	20,000	0.086	0.094	39.38	42.70
25	20,000	25,000	0.087	0.097	38.09	41.06	25,000	37,500	0.095	0.105	41.18	44.20
30	25,000	37,500	0.100	0.112	41.84	43.78	37,500	50,000	0.106	0.117	43.09	47.74

conditions indicates that the blockage is not just an inefficiency in fluid flow thru the filter (hydraulic), but also a broader threat to the mechanical and dynamic aspects of the piping system. As porosity tends to decrease, the flow is forced to pass thru the already reduced screen holes (perforations), resulting in high-velocity jets and potentially increasing turbulence.

This increased jet flow velocity will cause significant pressure changes on the filter surface and result in higher vibration amplitudes across all pressure drop levels. This behaviour aligns with recent CFD and FSI studies that prove the flow is confined above the hole surface, stabilising the fluid-structure interaction and amplifying the vibrations caused by increased jet-shear flow interaction (Li et al., 2023). The comparison between clean and clogged conditions shows a consistent increase in the ΔP - A relationship, indicating that clogging can generally enhance both hydraulic and vibrational dynamic reactions. A narrowed open area can create jet flow, strengthen shear layer instability, and lead to asymmetric vortex shedding, which ultimately can increase pressure and vibrational amplitude. Similar mechanisms were reported in high-fidelity turbulence studies (Shahzad et al., 2023) and FSI simulations of perforated structures (Kakroo & Sadat 2024).

This finding is very useful for oil and gas pipelines, where the conical strainer functions to filter and prevent the entry of particles, but can also increase ΔP and impact the increase in A (FIV). The strong relationship between ΔP and A It can be used as a basis for monitoring pressure changes as a predictive maintenance parameter. This is certainly consistent with a comprehensive evaluation of performance degradation, gradual damage, and the risk of failure caused by vibrations in the piping system (X. Zou et al., 2023). Therefore, optimizing optimising porosity and timely cleaning are crucial for maintaining operational reliability.

Frequency in clean and clogging conditions

The relationship between pressure drop and vibration frequency, caused by variations in porosity, cone angle, and hole pattern in clean and

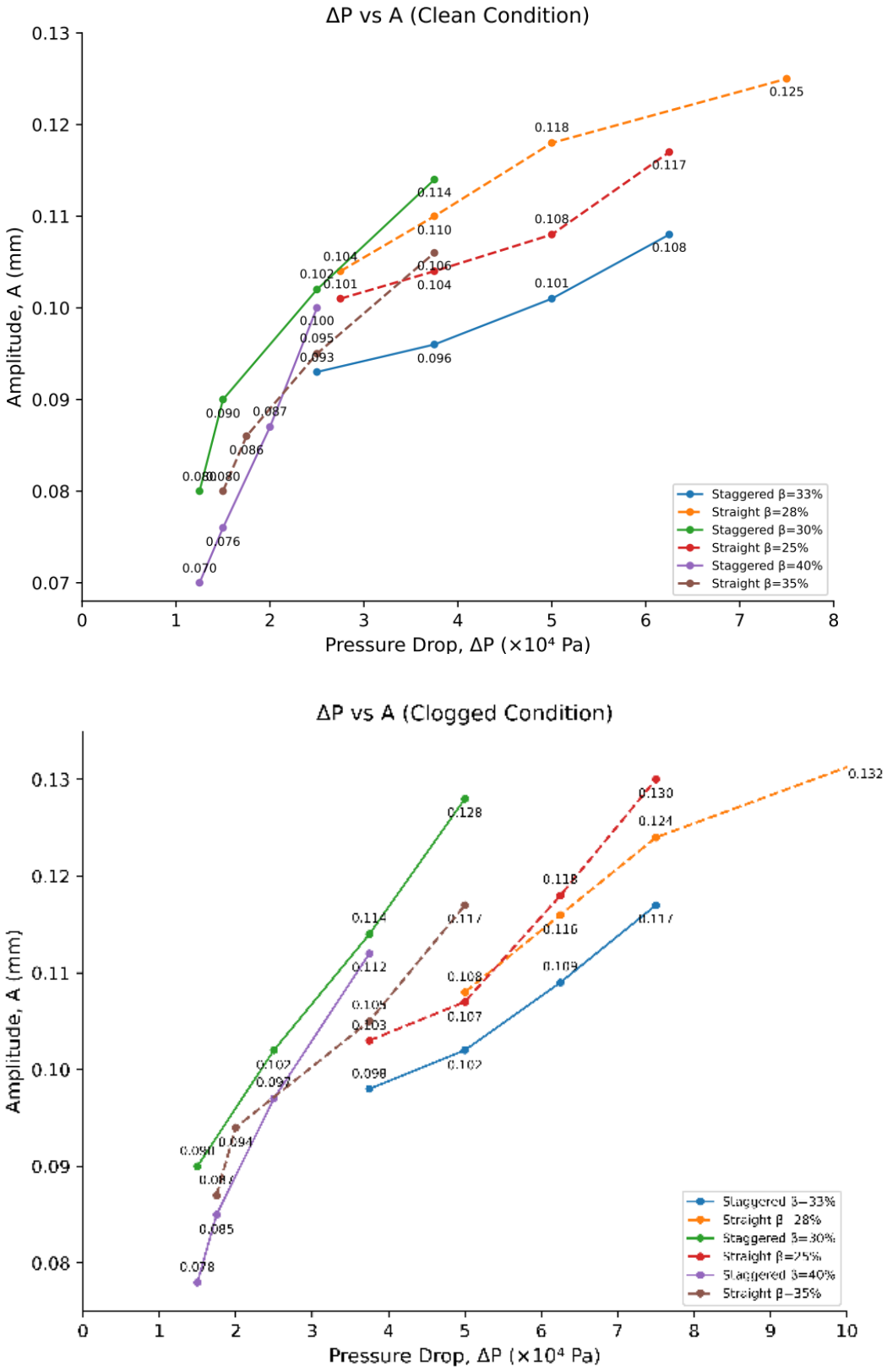

Figure 5. The effect of β and ΔP to A under clean and clogged conditions. Amplitude consistently increases with increasing pressure drop. Under clogged conditions, the response is more dominant than under clean conditions due to the intensification of hydrodynamic forces.

clogged conditions, is shown in Figure 6. Figure 6. The effect of β and ΔP to f under clean and clogged conditions. The ΔP - f relationship under clean and clogged conditions shows an increase in vibration frequency with increasing pressure drop, with a stronger dynamic response under clogged conditions. The relationship between ΔP and f in Figure 6 shows that an increase in pressure drop can also increase frequency. This occurs across all porosity configurations, both in clean and clogged conditions. This phenomenon illustrates the dynamic characteristic changes within the system. The increased frequency in the ΔP - f. The relationship occurs due to the control exerted by jet acceleration and turbulence intensity around the cone surface.

This indicates that the fluid flow has entered a faster vortex shedding regime. An increase in ΔP will increase the local flow velocity, hydrodynamically thru the energy relationship $U \approx \sqrt{(2\Delta P/\rho f)}$. Therefore, the jet velocity U inside the perforation increases with the addition of ΔP. This jet velocity directly affects the vortex shedding frequency fs thru the Strouhal number St, with the equation $fs = St(U/Deff)$. $Deff$ is the effective characteristic length (a combination of hole diameter, pitch, and perforation cluster). In this case, $Deff$=pitch (p) χ factor kluster (k) (Cicolin et al., 2024; Singh & Narasimhamurthy, 2022), so $fs = St.U/(k.p)$. The Strouhal number $St \approx 0{,}2$ (ROSHKO, 1955; Williamson, 1996) was used, and the value of k was obtained as shown in Table 4.

Table 4. Cluster factor (k) under both clean and clogged conditions.

β	k_{clean}	k_{clog}
30%	4.47	5.08
33%	7.56	8.48
40%	3.49	3.65
25%	6.05	6.49
28%	7.51	9.12
35%	3.71	3.88

Figure 7. Comparison of measurement frequency with equation-based predictions. This graph shows good agreement between the measured data and the predicted results under clean and clogged strainer conditions, with similar frequency trends at all test points. The difference between the two curves indicates the influence of experimental uncertainty and model simplification, but the main oscillation pattern is still successfully captured by the predictive approach.

Based on Figure 7, the measured frequency is on average 10.37% (10.35% under clean and 10.39% clogged conditions) lower than the predicted frequency, both in clean and clogged conditions. This difference is due to the simplified calculation of St, which does not fully account for multi-jet flow interactions, non-uniform blockage at each data point, and the FSI coupling inherent in the perforated cone geometry. However, the measured results have actually followed the current trend and the sequence of FIV responses at different levels of porosity. The same difference between experimental and predictive models for perforated structures was developed by (Li et al., 2024; Shahzad et al., 2022).

The experimental results show that the measured frequency ranges from (35-55 Hz), indicating that the dominant mechanism originates from the interaction of larger-scale vortices originating from the many collective jet-shear holes on the conical screen. The results of this study are consistent with the analysis of direct numerical simulation (DNS) and experiments on perforated structures (Shahzad et al., 2023).

The frequency increases sharply in clogged conditions compared to clean conditions. The effective porosity blockage is reduced, causing the flow to concentrate on specific paths. This condition results in concentrated jet flow, which exacerbates shear layer instability, increases coherent vortex shedding, and drives the system to increase its frequency. This change can create very energetic dynamics and accelerate the occurrence of resonance. Where the resulting frequency approaches the natural frequency of the structure, as studied by (Kakroo & Sadat 2024) in their report on the latest fluid-structure interaction on perforated plates.

In oil and gas pipeline systems, the measured frequency range (35-55 Hz) already includes the impermissible (High-Risk FIV Zone) because it represents a high-risk area due to flow (20-60 Hz) (E. Institute, 2008). Some parts that need attention

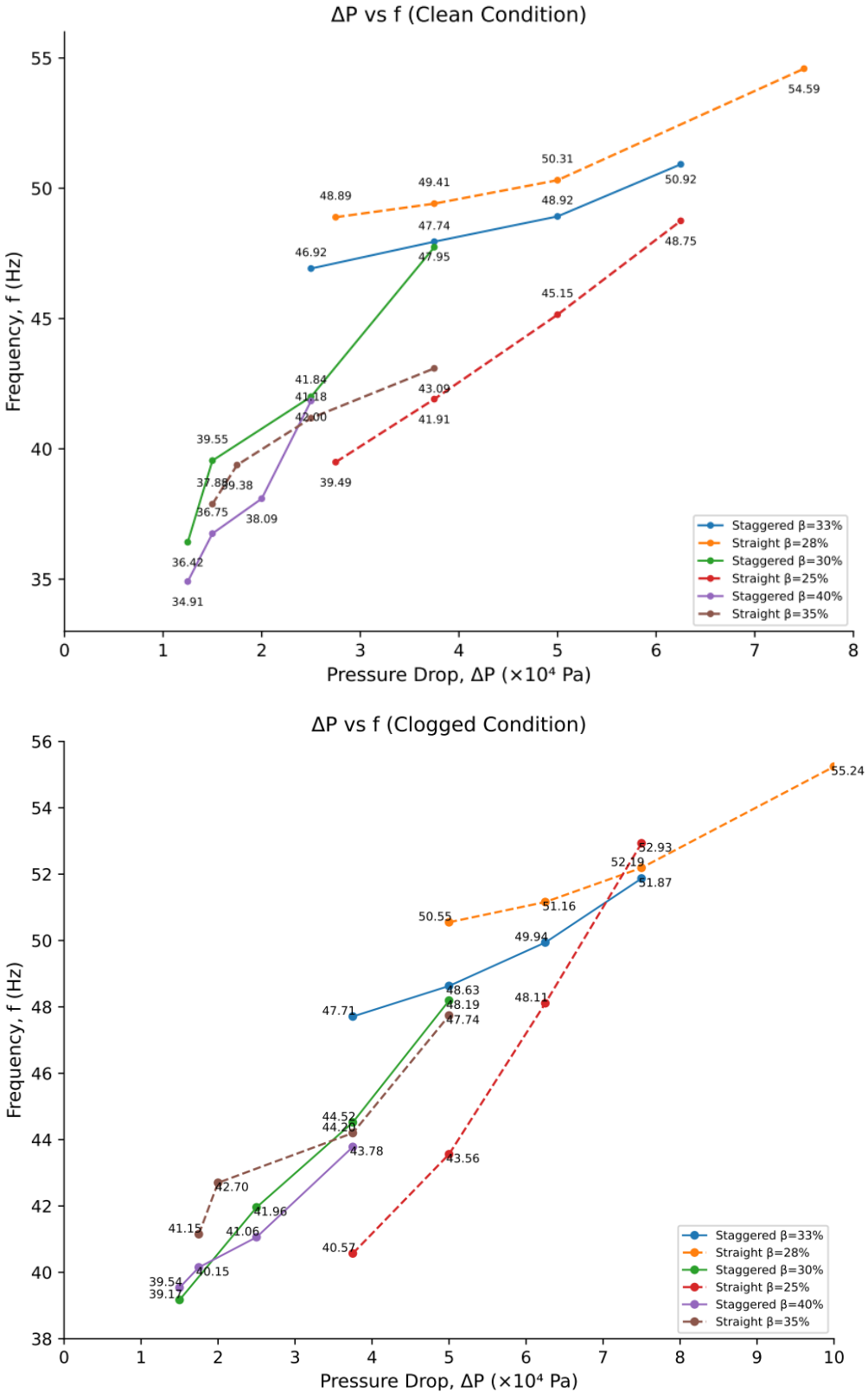

Figure 6. The effect of β and ΔP to f under clean and clogged conditions. The ΔP - f relationship under clean and clogged conditions shows an increase in vibration frequency with increasing pressure drop, with a stronger dynamic response under clogged conditions.

Thus, the frequency values shown in Figure 7 were obtained.

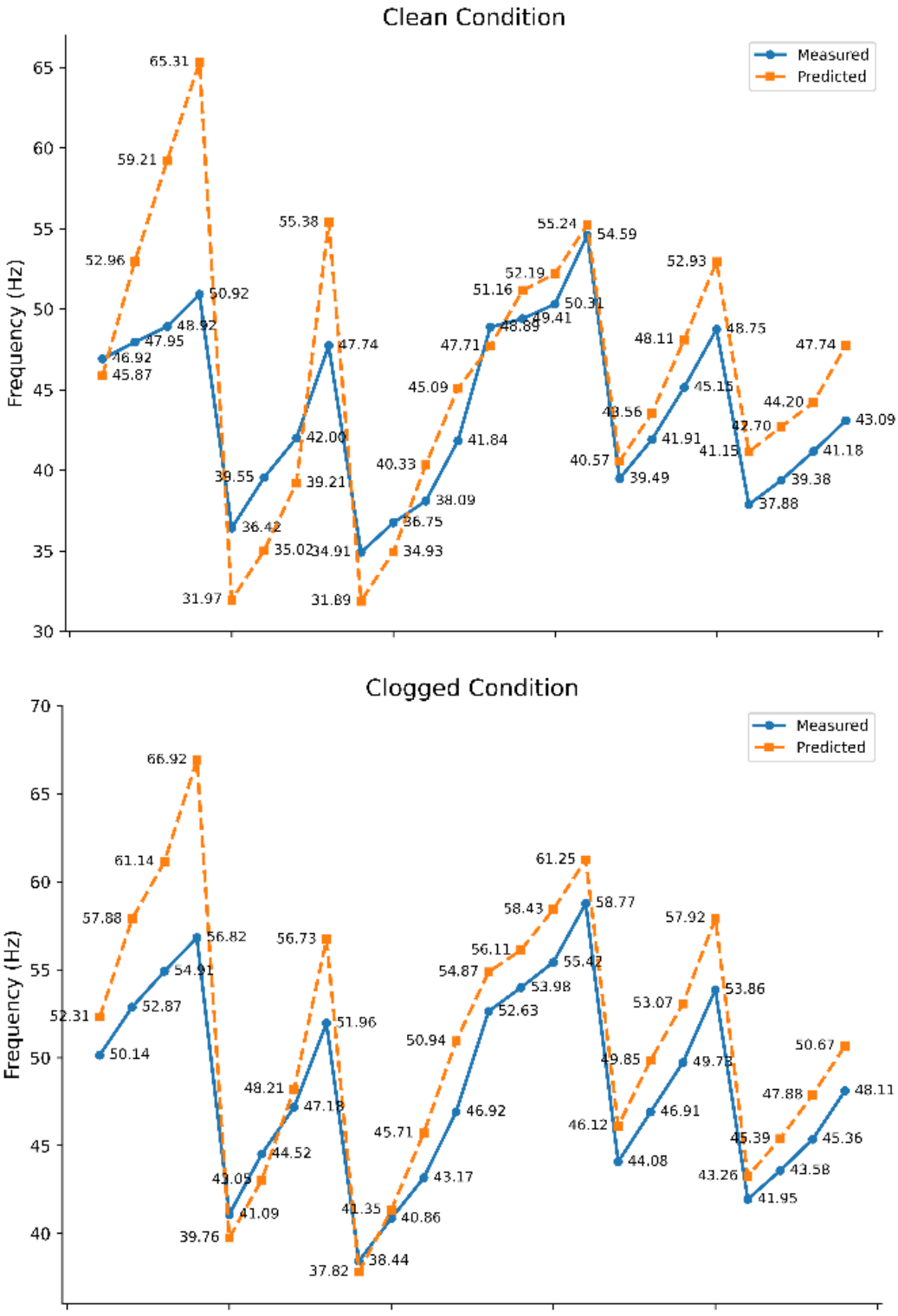

Figure 7. Comparison of measurement frequency with equation-based predictions. this graph shows good agreement between the measured data and the predicted results under clean and clogged strainer conditions, with similar frequency trends at all test points. the difference between the two curves indicates the influence of experimental uncertainty and model simplification, but the main oscillation pattern is still successfully captured by the predictive approach.

because this frequency range falls within the natural frequency of those parts, such as small-diameter connections (SDC), branch welds, thermal wells, and instrument tapping.

If left unchecked, this will lead to high-cycle fatigue and rapid crack propagation (A. P. Institute & of Mechanical Engineers 2021). This risk is further emphasised in the appendix (of Mechanical Engineers, 2020), which highlights the sensitivity of weld joints to dynamic stresses in the 20-60 Hz range.

Nondimensional flow-structure response.

Relationships between porosity β and nondimensional parameters $\bar{U}^*$, $\bar{A}/d$, and the scruton number (Sc) is shown in Table 5. The reduced velocity is defined as $\bar{U}^*=\bar{U}/(fd)$ and the Scruton number is given by $Sc=(2m\zeta)/(\rho f d^2)$. Where f is measured frequency, ζ is the structural damping ratio (for thin materials s=0,8 mm, it is assumed 0.005), $m=\rho s.s.b$ is structural mass per unit length. ρs is the density of material (Steel, 7850 kg/m^3), and b is unit width $\approx$ 1 m. The nondimensional parameters in Table 5 provide a deeper explanation of the flow-induced vibration (FIV) behaviour of conical strainers with varying porosity. Reduced velocity $\bar{U}^*$ exhibits a clear dependence on porosity: high-porosity configurations (e.g., Staggered β = 40%) show the lowest $\bar{U}^*_{\text{clean}}$=26.52, while low-porosity units (Straight β = 28%) reach $\bar{U}^*_{\text{clean}}$=64.05 . This trend intensifies under clogged conditions, with $\bar{U}^*_{\text{clog}}$ increasing by 10–20% across all series. This behaviour aligns with high-fidelity DNS studies of perforated plates, where reduced flow area amplifies jet velocity, shear-layer instability, and coherent vortex modes (Shahzad et al., 2022). The amplitude ratio $\bar{A}/d$ also increases with clogging, for example, from 0.033 to 0.036 (Staggered β=33%) and from 0.015 to 0.017 (Straight β=35%). This indicates that geometric choking amplifies the structural response, consistent with findings that local jet acceleration over perforated plates increases unsteady loading and flow oscillations (Celik & Rockwell, 2004; Dai, 2020; Shahzad et al., 2022).

The observed increase in $\bar{A}/d$ is consistent with classical cylinder-based FIV scaling, where oscillation magnitude grows with wake asymmetry and jet-shear interaction (E. Institute 2008).

Scruton numbers for all series fall within Sc= 2.19 -8.79, well below the $Sc\geq$ 10 threshold recommended by ASME/API for vibration-resistant thin-shell components. Low Scruton values indicate high susceptibility to excitation due to limited mass-damping capacity.

Similar thresholds for piping vibration risk are reported in (E. Institute, 2008) for dynamic interaction failures in process facilities. Using $Sc=(2m\zeta)/(\rho f d^2)$, the extremely low damping ratio of thin steel strainers ($\zeta\approx0.005$) places the components in the *high-risk* regime, especially when porosity decreases due to clogging.

Collectively, these nondimensional indicators quantitatively reinforce earlier $\Delta P - A$ and $\Delta P - f$ results: Clogging not only increases hydraulic

Table 5. Nondimensional parameters (clean vs clogged)

Hole pattern, β	$\bar{U}_{clean}$	$\bar{U}_{clog}$	$\bar{U}^*_{clean}$	$\bar{U}^*_{clog}$	$\frac{\bar{A}_{clean}}{d}$	$\frac{\bar{A}_{clog}}{d}$	Sc
Stag, 30%	6.72	7.80	40.54	46.00	0.024	0.027	4.92
Stag, 33%	9.37	10.62	64.15	71.48	0.033	0.036	8.79
Stag, 40%	6.03	6.90	26.52	27.97	0.014	0.012	2.19
Stra, 25%	9.44	10.62	53.82	57.37	0.027	0.029	4.92
Stra, 28%	9.76	12.06	64.05	76.88	0.038	0.040	8.75
Stra, 35%	6.90	7.92	28.49	30.03	0.015	0.017	2.19

resistance but shifts the strainer toward a dynamically unstable operating regime, validating the proposed porosity-sensitivity mechanism. This coupled hydraulic-structural amplification provides a clear explanation for the 10–20% vibration increase observed experimentally and highlights the importance of porosity management in oil and gas pipeline protection systems.

Influence of porosity (β) on clogging factor (CF)

The clogging factor (CF) is used to assess the level of clogging in a conical screen by comparing the differential pressure between clean and clogged conditions, see equation 3. The experimental results show that porosity has a dominant influence on the magnitude of CF, while the perforation pattern acts as a supporting factor, as illustrated in Figure 9. Figure 9 shows that conical strainer with lower porosity (β≥30%) experience significantly higher clogging factors, indicating severe geometric clogging that intensifies jet contraction, turbulent friction, and early particle accumulation.

This behaviour aligns with recent findings regarding turbulence amplification on low-permeability perforated plates (Shahzad et al., 2022) and jet-induced oscillatory loading (Celik & Rockwell, 2004). The resulting flow acceleration increases flow-induced vibration (FIV) and raises structural stress under FSI coupling, where as designs with higher porosity and staggered patterns (β ≥35%) reduce unstable pressure fluctuations and suppress resonance paths, consistent with geometric-based attenuation mechanisms (Dai 2020). Overall, the configuration with a larger cone angle (θ = 81°), intermittent perforations, and porosity ≥ 35% offers superior hydraulic stability and a lower risk of vibration, making it the most reliable choice for oil and gas filtration applications.

Practical implications for oil and gas exploration and exploitation

In oil and gas exploration and exploitation activities, the findings of this study have significant implications, particularly for the pipeline system where the conical strainer is installed upstream and downstream. Pumps, compressors, and other process equipment can be protected from contamination by solid dirt. Field conditions during the drilling process, initial production, well testing, and mature field exploitation will experience fluctuating flow rates, the presence of entrained solids, and progressive plugging. Filters with medium to high porosity in an alternating perforation pattern consistently exhibit lower clogging factors, reduced pressure drop, and more stable vibration response compared to low porosity.

Filters in piping systems with low porosity and under partially clogged conditions will cause flow-induced vibration (FIV) due to accelerated jet flow and increased turbulence. Therefore, this study also confirms that screen porosity is a parameter that can prevent vibration. Failures in oil and gas facilities generally occur at weld joints, small-diameter connections, and instrumentation branches. The immediate consequences received can include operational shutdowns and can lead to production losses (Emmerson et al., 2020; X. Zou et al., 2023).

Therefore, improper selection of porosity significantly affects the increased operational risks during both the exploration and long-term exploitation processes. For operators, selecting the right porosity can reduce maintenance frequency and improve equipment availability, especially in offshore and remote areas. Preventive maintenance is also required, including periodic observation of pressure drops. This approach strongly supports risk-based maintenance strategies and aligns with industry-recognised vibration management practices (Celik & Rockwell 2004; Shahzad et al., 2022).

CONCLUSION

This study concludes that porosity plays a significant role in regulating flow instability and vibration behaviour in a conical strainer. The experimental results show that the straight configuration with low porosity experiences intense geometric constriction, which promotes the formation of high-speed jets, stronger shear layer disturbances, and an increase in vibration amplitude as blockage progresses.

However, conversely, screens with a porosity greater than or equal to 30% and staggered perforations can maintain finer flow dispersion,

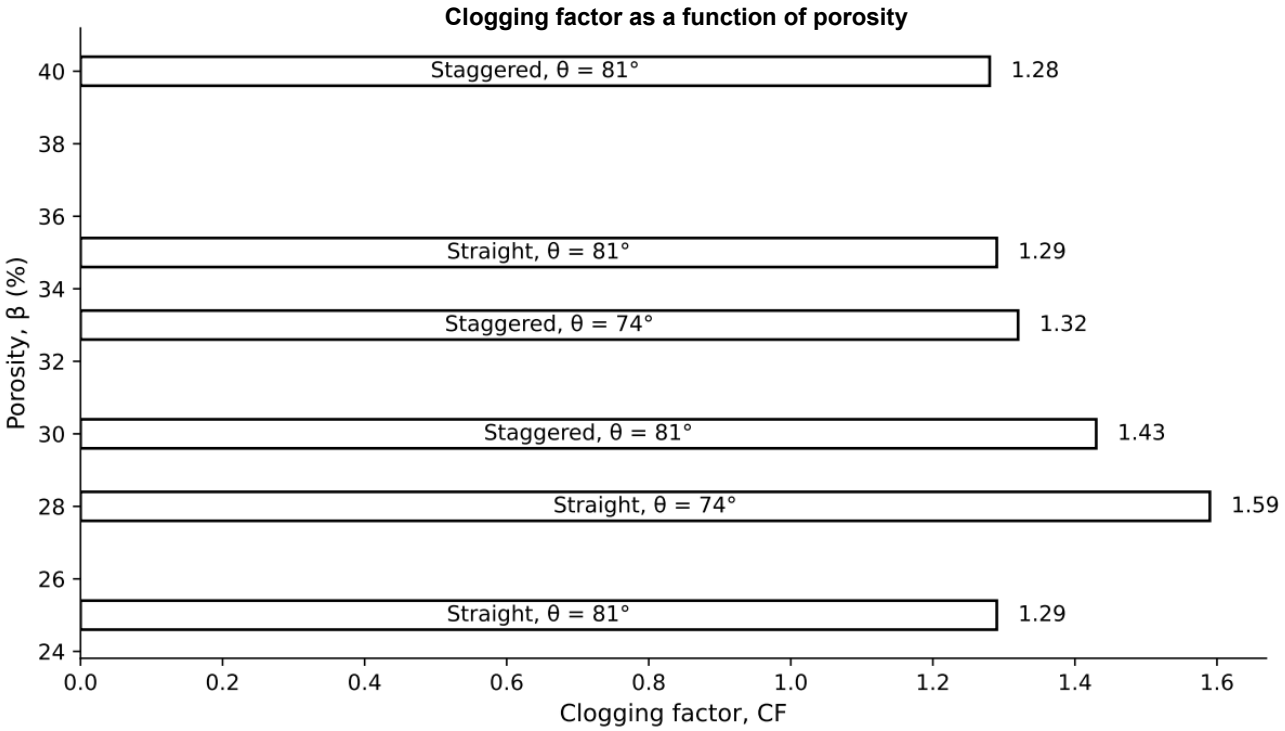

Figure 9. Clogging factor as a function of strainer porosity and hole configuration. This graph illustrates the relationship between porosity and the clogging factor for various cone strainer configurations, showing that a decrease in porosity and variations in perforation geometry significantly increase the tendency for clogging.

reduce the occurrence of increased pressure drop, and provide more stable vibration response. This confirms that this type of conical screen design has greater resistance to flow instability caused by clogging. By integrating pressure drop measurements, vibration metrics including amplitude and frequency, and fouling behavior behaviour within a unified framework, this research addresses a long-standing gap in the literature where the interaction between hydraulic performance and FIV behaviour on conical screens has not been quantitatively demonstrated. The relevance of these findings to oil and gas operations highlights the importance of developing cone filters that are resistant to the hydraulic loads and vibrations caused by flow. The relationship shown between porosity, flow instability, and vibration response indicates that future research should focus on the structural behaviour of the screen due to high-velocity jets, unstable pressure fields, and progressive clogging. Using FSI modelling, the CFD-FEA approach is highly anticipated in predicting the design of conical strainers that are resistant to deformation and structural cracking, thus maintaining filtration capability during long-term operation in piping systems.

ACKNOWLEDGEMENT

The authors would like to express their gratitude to the Department of Mechanical Engineering at Politeknik Caltex Riau in Indonesia and the Faculty of Mechanical and Manufacturing Engineering at Universiti Tun Hussein Onn Malaysia for providing access to laboratories, technical assistance, and academic guidance during this research. These two collaborating institutions are very important in ensuring the successful completion of this research. The author would also like to express gratitude to the parties who assisted in the completion of this paper, including T. Muhammad Ferdi and Muhammad Zul Idzham bin Abdul Ghani.

GLOSSARY OF TERMS

Symbol	Defenition	Unit
ρ	Density	kg/m^3
μ	Dynamic viscosity	$Pa.s$
T	Terperature	℃
Q	Flow rate	m^3/h

Re	Reynolds number	–
β	Porosity	%
θ	Cone angle	Deg
d	Hole diameter	mm
D	Internal Pipe diameter	mm
L	Strainer length	mm
p	Hole Pitch	mm
$v(t)$	Velocity	mm/s
$a(t)$	Acceleration	m/s^2
$x(t)$	Displacement	mm
A	Amplitude	mm/s
f	Frequency	mm
ΔP	Pressure Drop	Hz
CF	Clogging factor	Pascal
St	Strouhal Number	–
D_{eff}	Effective characteristic length	Mm
k	Cluster Factor	–
U	Jet Velocity	m/s

REFERENCE

Akhyan, A., Hussein, M. D., & Bin Razali, M. A. (2025). Influence of Installation Orientation and Cone Angle on Pressure Drop and Filtration Efficiency of Conical Strainers. Scientific Contributions Oil and Gas, 48(3), 303–320. https://doi.org/10.29017/scog.v48i3.1910

Bon, G., Chatellier, L., Le Guer, Y., Bellot, C., Casiot, X., & David, L. (2024). Pressure Loss Modeling for Multi-Stage Obstacles in Pressurized Ducts. Energies, 17(14). https://doi.org/10.3390/en17143505

Carlomagno, M., Rossin, S., Delvecchio, M., & Anichini, A. (2012). Experimental and Numerical Validation of Conical Strainer Fluid/ Structural Performance Model. Proceedings of the ASME Turbo Expo, 6. https://doi.org/10.1115/GT2012-69751

Celik, E., & Rockwell, D. (2004). Coupled oscillations of flow along a perforated plate. Physics of Fluids, 16(5), 1714–1724. https://doi.org/10.1063/1.1661625

Chu, T., Nguyen, T., Yoo, H., & Wang, J. (2024). A review of vibration analysis and its applications. Heliyon, 10(5), e26282. https://doi.org/https://doi.org/10.1016/j.heliyon.2024.e26282

Cicolin, M. M., Chellini, S., Usherwood, B., Ganapathisubramani, B., & Castro, I. P. (2024). Vortex shedding behind porous flat plates normal to the flow. Journal of Fluid Mechanics, 985, A40. https://doi.org/DOI: 10.1017/jfm.2024.300

Dai, X. (2020). Flow–acoustic resonance in a cavity covered by a perforated plate. Journal of Fluid Mechanics, 884, A4. https://doi.org/DOI: 10.1017/jfm.2019.934

Eker, O. F. (2014). Physics-Based Degradation Modelling for Filter Clogging. Cranfield University.

Emmerson, P. R., Lewis, M. J., Barton, N. A., Orre, S., & Lunde, K. (2020, August 3). Flow Induced Vibration Analysis of Topside Piping at High Pressure. Volume 8: CFD and FSI. https://doi.org/10.1115/OMAE2020-18760

Ergut, A. (2025). Analysis of Transverse Vibration in a Concentrated Mass Rayleigh Pipe. Symmetry, 17(3). https://doi.org/10.3390/sym17030371

Fang, W., Chen, S., Li, S., & Zuriguel, I. (2024). Clogging transition of granular flow in porous structures. Physical Review Research, 6 (3). https://doi.org/10.1103/PhysRevResearch.6.033046

Fuad, M. F. I. A., Lukman, N., & Nazari, A. D. Z. A. (2019). Flow induced vibration (FIV) research of oil and gas process piping system. International Journal of Recent Technology and Engineering, 8(2 Special Issue 8), 1387–1390. https://doi.org/10.35940/ijrte.B1072.0882S819

Hamzah, K., Yasutra, A., & Irawan, D. (2021). Prediction of Hydraulic Fractured Well Performance Using Empirical Correlation and Machine Learning. Scientific Contributions Oil and Gas, 44, 141–152. https://doi.org/10.29017/SCOG.44.2.589

Harper, C., Bibby, C., Hartford, N., Harris, C., & Popa, C. (2024, November). Flow-Induced Vibration Assessment and Mitigation for Compressor Station Expansion. https://doi.org/10.1115/IPC2024-133362

Inservice Testing of Pumps in Light-Water Reactor Power Plants (Issue ASME OM-3:2022). (2022). ASME.

Institute, A. P., & of Mechanical Engineers, A. S. (2021). API 579-1/ASME FFS-1: Fitness for Service (3rd ed.). API / ASME.

Institute, E. (2008). Guidelines for the Avoidance of Vibration Induced Fatigue Failure in Process Pipework (2nd ed.). Energy Institute.

Kakroo, K., & Sadat, H. (2024). High-fidelity fluid –structure interaction simulations of perforated elastic vortex generators. Physics of Fluids, 36 (11), 113608. https://doi.org/10.1063/5.0234900

Li, S., Davidson, L., & Peng, S.-H. (2023). A fluid flow model for the pressure loss through perforated plates. http://arxiv.org/abs/2304.11730

Li, S., Davidson, L., & Peng, S.-H. (2024). A pressure-loss model for flow-through round-hole perforated plates of moderate porosity and thickness in laminar and turbulent flow regimes. International Journal of Heat and Mass Transfer, 226, 125490. https://doi.org/10.1016/j.ijheatmasstransfer.2024.125490

Mahajan, G. P., & Maurya, R. S. (2020). Development of an Efficient T-type Strainer With its Performance Evaluation. In Journal of Thermal Engineering (Vol. 6, Issue 6). Yildiz Technical University Press.

Measurement of fluid flow in closed conduits – Guidance to the selection, installation and use of Coriolis meters (mass flow, density and volume flow measurements) (Issue ISO 10790:2015). (2015). ISO.

Mechanical vibration – Evaluation of machine vibration by measurements on non-rotating parts – Part 3: Industrial machines with nominal power above 15 kW and nominal speeds between 120 r/min and 15 000 r/min when measured in situ (Issue ISO 10816-3:2022). (2022). ISO.

Mechanical vibration – Requirements for instruments for measuring vibration severity (Issue ISO 2954:2012). (2012). ISO.

Mironovs, V., Osipova, M., Akishin, P., Zemchenkovs, V., & Serdjuks, D. (2025). Methods for Evaluating the Elastic Properties of Stainless Steel Perforated Plates. Metals, 15(7). https://doi.org/10.3390/met15070711

of Mechanical Engineers, A. S. (2020). ASME B31.3: Process Piping (including Appendix F – Guidance and Precautionary Considerations) (2020th ed.). ASME Press.

Pressure gauges – Part 1: Bourdon tube pressure gauges (Issue EN 837-1:1996). (1996). CEN.

Puderbach, V., Schmidt, K., & Antonyuk, S. (2021). A coupled CFD-DEM model for resolved simulation of filter cake formation during solid-liquid separation. Processes, 9(5). https://doi.org/10.3390/pr9050826

Qiao, S., Li, J., Ren, J., & Kim, S. (2023). Experimental Investigation on Effects of Flow Orientation on Interfacial Structure of Air–Water Two-Phase Flow. Coatings, 13(1). https://doi.org/10.3390/coatings13010005

Qing, M., Jinghui, Z., Yushan, L., Haijun, W., & Quan, D. (2006). Experimental studies of orifice -induced wall pressure fluctuations and pipe vibration. International Journal of Pressure Vessels and Piping, 83(7), 505–511. https://doi.org/https://doi.org/10.1016/j.ijpvp.2006.03.010

Rianto, R., Akhyan, A., Novison, R., Yanda Zaira, J., Haiqal Jurusan Teknik Mesin, M., & Caltex Riau Jl Umbansari No, P. (2025). Studi Numerik Penurunan Tekanan (ΔP) Akibat Perubahan Sudut (θ), Tipe Lubang dan Open Rasio Area (OAR) Pada Strainer (Vol. 05, Issue 01).

ROSHKO, A. (1955). On the Wake and Drag of Bluff Bodies. Journal of the Aeronautical Sciences, 22(2), 124–132. https://doi.org/10.2514/8.3286

Segismundo, N. R., Alejo, L. A., & Mays, D. C. (2017). A Laboratory Study on the Filtration and Clogging Behaviour of Filter Media. Water, 9(8), 583. https://doi.org/10.3390/w9080583

Shady, O., Renno, J., Mohamed, M. S., Sassi, S., & Muthalif, A. (2022). On the Suitability of Vibration Acceptance Criteria of Process Pipework. Advances in Materials Science and Engineering, 2022, 1–9. https://doi.org/10.1155/2022/2168818

Shahzad, H., Hickel, S., & Modesti, D. (2022). Permeability and Turbulence Over Perforated Plates. Flow, Turbulence and Combustion, 109, 1–14. https://doi.org/10.1007/s10494-022-00337-7

Shahzad, H., Hickel, S., & Modesti, D. (2023).

Turbulence and added drag over acoustic liners. Journal of Fluid Mechanics, 965, A10. https://doi.org/DOI: 10.1017/jfm.2023.397

Singh, A., & Narasimhamurthy, V. D. (2022). Perforation effects on the wake dynamics of normal flat plates. Journal of Fluid Mechanics, 947, A23. https://doi.org/DOI: 10.1017/jfm.2022.646

Suhaib, K. H., & Bhunia, P. (2023). Clogging index: A tool to quantify filter bed clogging in horizontal subsurface flow macrophyte-assisted vermifilter. Water Environment Research, 95 (1), e10821. https://doi.org/10.1002/wer.10821

Wang, H., Wu, J., Fu, P., Qu, Z., Zhao, W., & Song, Y. (2022). CFD-DEM Study of Bridging Mechanism of Particles in Ceramic Membrane Pores under Surface Filtration Conditions. Processes, 10(3). https://doi.org/10.3390/pr10030475

Wang, T., & Li, M. (2025). Particle migration and pore clogging in porous media during supercritical carbon dioxide sequestration. Computers and Geotechnics, 185. https://doi.org/10.1016/j.compgeo.2025.107316

Wayo, D. D. K., Irawan, S., Khan, J. A., & Fitrianti. (2022). CFD Validation for Assessing the Repercussions of Filter Cake Breakers; EDTA and SiO2 on Filter Cake Return Permeability. Applied Artificial Intelligence, 36 (1). https://doi.org/10.1080/08839514.2022.2112551

Widarsono, B. (2022). Uji Coba Teknik Baru untuk Menentukan Parameter Pancung Porositas Pada Kasus Reservoir Batugamping. Lembaran Publikasi Minyak Dan Gas Bumi, 44, 1–11. https://doi.org/10.29017/LPMGB.44.1.151

Williamson, C. H. K. (1996). Vortex Dynamics in the Cylinder Wake. Annual Review of Fluid Mechanics, 28(Volume 28, 1996), 477–539. https://doi.org/https://doi.org/10.1146/annurev.fl.28.010196.002401

Yin, Y., Cui, Y., & Jing, L. (2024). Clogging and Unclogging of Fine Particles in Porous Media: Micromechanical Insights From an Analog Pore System. Water Resources Research, 60(1). https://doi.org/10.1029/2023WR034628

Zou, X., Xie, B., Zang, Z., Chen, E., & Hou, J. (2023). Vortex-Induced Vibration and Fatigue Damage Assessment for a Submarine Pipeline on a Sand Wave Seabed. Journal of Marine Science and Engineering, 11(10). https://doi.org/10.3390/jmse11102031

Zou, Y., Du, Y., Zhao, Z., Pang, F., Li, H., & Hui, D. (2024). Experimental and Simulation Study on Flow-Induced Vibration of Underwater Vehicle. Journal of Marine Science and Engineering, 12(9). https://doi.org/10.3390/jmse12091597